Journal of Medicinal Chemistry

pubs.acs.org/jmc

Article

Lead Optimization of Butyrolactone I as an Orally Bioavailable Antiallergic Agent Targeting FcγRIIB

Chun-Lan Xie,[#] Hong-Xiu Xiao,[#] Pei-Fang Song,[#] Qing-Mei Liu,[#] Haoxiang Wei, Liang Wu, Guang-Hao Zhu, Guang-Ming Liu,[*] Yandong Zhang,[*] Ping Wang,[*] and Xian-Wen Yang[*]

Cite This: *J. Med. Chem.* 2024, 67, 7504−7515

Read Online

ACCESS | Metrics & More | Article Recommendations | Supporting Information

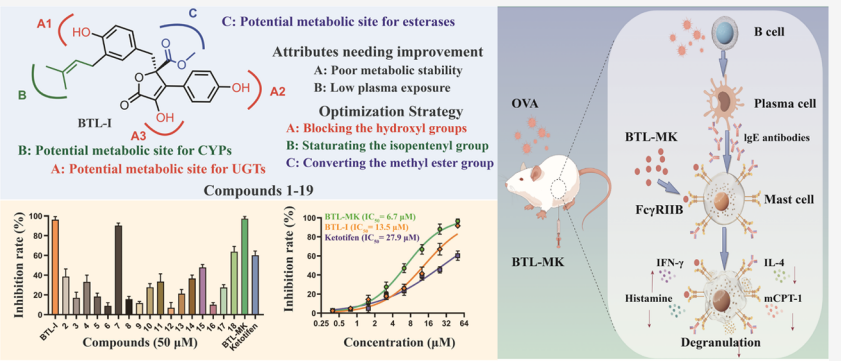

ABSTRACT: Food allergy (FA) poses a growing global food safety concern, yet no effective cure exists in clinics. Previously, we discovered a potent antifood allergy compound, butyrolactone I (BTL-I, **1**), from the deep sea. Unfortunately, it has a very low exposure and poor pharmacokinetic (PK) profile in rats. Therefore, a series of structural optimizations toward the metabolic pathways of BTL-I were conducted to provide 18 derives (**2**−**19**). Among them, BTL-MK (**19**) showed superior antiallergic activity and favorable pharmacokinetics compared to BTL-I, being twice as potent with a clearance (CL) rate of only 0.5% that of BTL-I. By oral administration, C_{max} and area under the concentration−time curve ($AUC_{0-\infty}$) were 565 and 204 times higher than those of BTL-I, respectively. These findings suggest that butyrolactone methyl ketone (BTL-BK) could serve as a drug candidate for the treatment of FAs and offer valuable insights into optimizing the druggability of lead compounds.

INTRODUCTION

Food allergies (FAs) are adverse immune reactions to food proteins that can cause a range of clinical symptoms affecting various bodily systems,[1] including the skin,[2] respiratory,[3] gastrointestinal,[4,5] cardiovascular,[6] and nervous systems.[7] The prevalence of FAs has dramatically increased over the recent decades, leading to a rise in hospitalizations for food-induced anaphylaxis, representing what appears to be the "second wave of the allergy epidemic" after the surge in the prevalence of asthma and respiratory allergy in previous decades.[8] The World Health Organization (WHO) recognizes FA as a significant public health issue, affecting approximately 5% of adults and 8% of children and significantly impacting their lives.[9]

Currently, there is no cure for FAs, and the main approach to management is allergen avoidance.[10] However, complete avoidance of allergenic proteins in the diet is challenging, particularly in children's diets.[11,12] As a result, it is crucial to have emergency medication available to treat acute allergic reactions that may arise from accidental exposure to allergens, which, unfortunately, is common. Antihistamines, steroids and nonsteroids, and epinephrine are the three main medications used to alleviate FA.[13,14] However, these medications have several limitations, including being unsuitable for children under 2 years old, having numerous side effects, and potentially fatal if misused. Therefore, improving therapeutic options has become vital for food allergy research.

The mechanisms underlying FAs are complex, and the breakdown of immunologic and clinical tolerance to an ingested food is a common mechanism leading to various food allergies, resulting in either immunoglobulin E (IgE)-mediated reactions or non-IgE-mediated disorders.[15] T cells play a central role in coordinating the immune response to food allergens, specifically by stimulating the production of antibodies by B cells. Recent studies have highlighted the role of basophils and mast cells (MCs) in allergic reactions to

Received: February 8, 2024
Revised: April 6, 2024
Accepted: April 10, 2024
Published: April 19, 2024

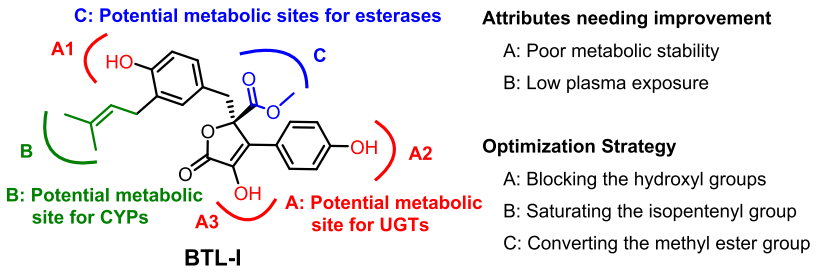

Figure 1. Profile overview of BTL-I and considerations for the optimization strategy.

Scheme 1. Modification of Hydroxy Groups of BTL-I

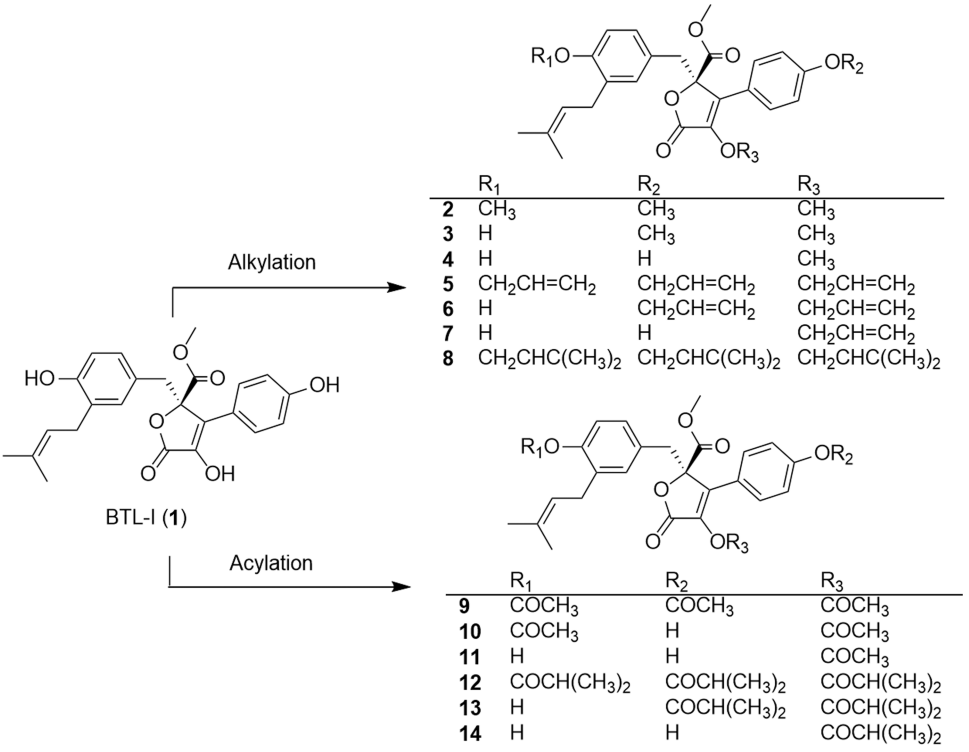

	R_1	R_2	R_3
2	CH_3	CH_3	CH_3
3	H	CH_3	CH_3
4	H	H	CH_3
5	$CH_2CH{=}CH_2$	$CH_2CH{=}CH_2$	$CH_2CH{=}CH_2$
6	H	$CH_2CH{=}CH_2$	$CH_2CH{=}CH_2$
7	H	H	$CH_2CH{=}CH_2$
8	$CH_2CHC(CH_3)_2$	$CH_2CHC(CH_3)_2$	$CH_2CHC(CH_3)_2$

	R_1	R_2	R_3
9	$COCH_3$	$COCH_3$	$COCH_3$
10	$COCH_3$	H	$COCH_3$
11	H	H	$COCH_3$
12	$COCH(CH_3)_2$	$COCH(CH_3)_2$	$COCH(CH_3)_2$
13	H	$COCH(CH_3)_2$	$COCH(CH_3)_2$
14	H	H	$COCH(CH_3)_2$

foods.[16−18] MCs are one of the fastest immune cell responders, releasing mediators such as histamine, serotonin, cytokines, and proteases from intracellular stores upon cross-linking of Fc epsilon region receptor 1 (FcεR1)-bound IgE with allergens.[19] Therefore, targeting MCs may be a promising strategy for treating allergic disorders. Inhibiting MCs activation requires coaggregation of Fc receptor IIB for IgG (FcγRIIB) with FcεRI, which makes developing ligands for FcγRIIB of great significance in inhibiting MC activation.[20,21]

In our previous study, we discovered that deep-sea-derived butyrolactone I (BTL-I) isolated from *Aspergillus* sp. can reduce the levels of histamine and mouse mast cell proteinases by binding to the inhibitory receptor FcγRIIB.[20] However, the low exposure and poor pharmacokinetic (PK) profile of BTL-I in rats limited its applications *in vivo*.[22] This suboptimal PK behavior could be attributed to rapid first-pass metabolism in the liver. Therefore, during the lead optimization program, we attempted to improve BTL-I exposure *in vivo* by slowing its first-pass metabolism while preserving its antiallergenic activity. In this study, the structural optimization strategy of the FcγRIIB inhibitors based on the lead compound BTL-I with simultaneous improvement of metabolic stability and pharmacodynamic activity was described. The findings indicated that the optimized compound (BTL-MK, **19**) exhibited potent antiallergic activity *in vitro* and *in vivo*, along with favorable oral exposure in rats. These results suggest that it has the potential to deliver a candidate drug for FAs.

RESULTS AND DISCUSSION

Optimization Strategy. The key issue for BTL-I was low exposure in rats, coupled with a poor PK profile. Hence, our focus was on improving the suboptimal physicochemical properties and poor PK profile of BTL-I while maintaining its high on-target potency. To address this challenge, we first characterized the main metabolic pathways of BTL-I in rats, which include hydrolysis, oxidation, and glucuronidation. With these data in hand, we developed a structural optimization strategy that focused on three main metabolic pathways (Figure 1).[23−26] The first optimization strategy was to improve the tolerance of BTL-I to UDP-glucuronosyltransferases by modifying the chemical environments of hydroxyl groups of BTL-I. This was achieved by shielding the hydroxyl groups in parts A1−A3 through alkylation or esterification. Second, the isopentene chain in part B was optimized by a reduction or cyclization reaction. Third, the methyl carboxylate group was replaced by other oxygen-containing functional groups to

https://doi.org/10.1021/acs.jmedchem.4c00354
J. Med. Chem. 2024, 67, 7504−7515

Scheme 2. Modification of the Isopentene Group of BTL-I

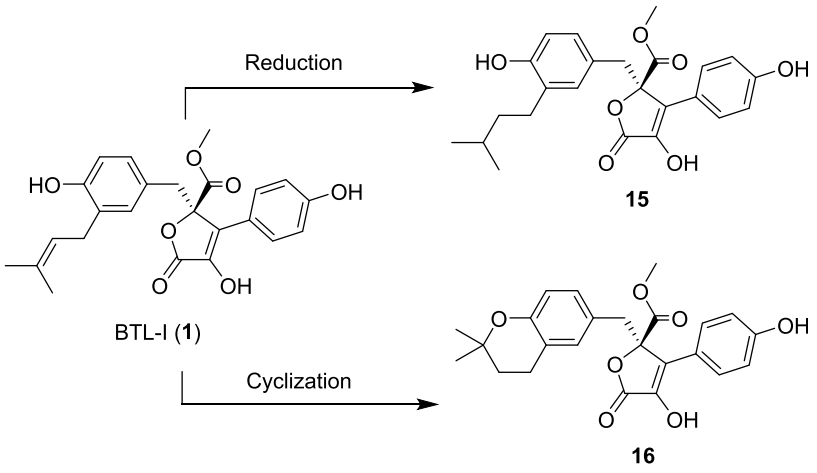

Scheme 3. Modification of the Ester Group of BTL-I

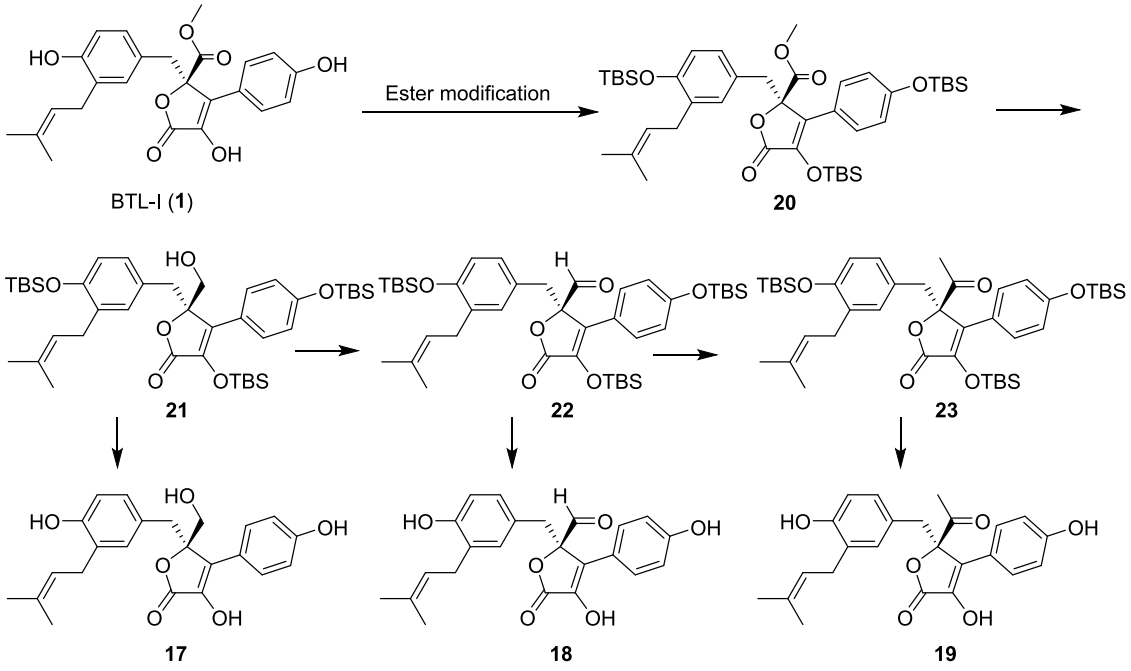

improve its tolerance to esterases. This comprehensive optimization strategy was designed to simultaneously enhance the metabolic stability and biological activity of lead compound BTL-I.

Chemistry. A series of BTL-I derivatives were designed and synthesized considering the ligand binding ability assessment and the BTL-I metabolite profile. The hydroxyl groups of BTL-I were initially partially or fully blocked by alkylation and acylation reactions (Scheme 1). Alkylation of BTL-I with methyl iodide (**2**, yield 25%; **3**, yield 58%; **4**, yield 48%), 1-bromo-3-methyl-2-butene (**5**, yield 9%; **6**, yield 62%; **7**, yield 15%), and allyl bromide (**8**, yield 54%) afforded the corresponding ether derivatives (**2**−**8**). Acetylation with acetyl chloride (**9**, yield 1%; **10**, yield 14%; **11**, yield 15%) and 2-methylpropionyl chloride (**12**, yield 13%; **13**, yield 11%; **14**, yield 1%) resulted in ester derivatives (**9**−**14**).

Next, the isopentene group of BTL-I was saturated with palladium carbon and H_2 to give compound **15** (yield 68%). Intramolecular cyclization in the presence of HCl delivered pyrane compound **16** (yield 66%) (Scheme 2).

Finally, the methyl carboxylate group was converted to the corresponding alcohol (**17**), aldehyde (**18**), and methyl ketone (**19**), as shown in Scheme 3. After global protection of hydroxyl groups of BTL-I with *tert*-butyldimethylsilyl (TBS) (yield 74%), the ester group was selectively reduced by lithium borohydride to afford alcohol **21** (yield 71%). Subsequent oxidation with Dess−Martin reagent generated aldehyde **22** (yield 57%). The aldehyde **22** was sequentially treated with trimethylaluminum and Dess−Martin Reagent to afford methyl ketone **23** (yield 19%). The removal of the TBS groups in **21**, **22**, and **23** with *tetra-n*-butylammonium fluoride delivered alcohol (**17**, yield 92%), aldehyde (**18**, yield 77%), and methyl ketone (BTL-MK, **19**, yield 74%).

***In Vitro* Antiallergic Activities of BTL-I Derivatives.** To assess the potency of the BTL-I derivatives as antiallergy, their inhibition rate of degranulation was determined using an IgE-mediated RBL-2H3 cell model.[27,28] The level of *β*-

https://doi.org/10.1021/acs.jmedchem.4c00354
J. Med. Chem. 2024, 67, 7504−7515

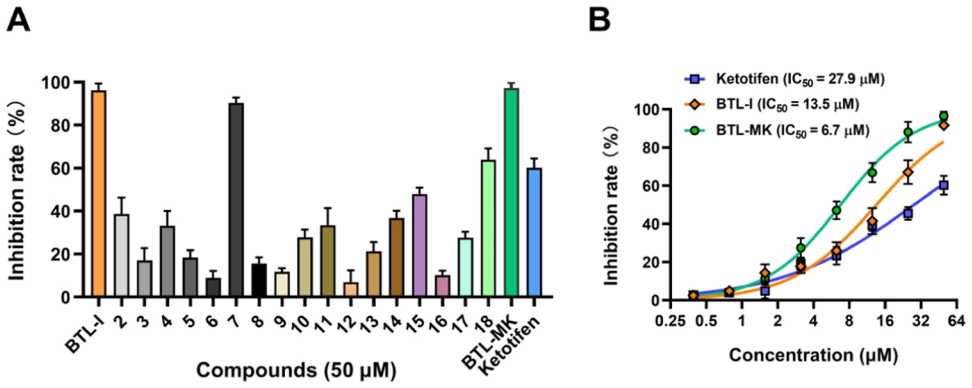

Figure 2. Antiallergic activities of BTL-I derivatives. (A) Inhibition rate of degranulation of BTL-I derivatives at 50 μM. (B) Dose-dependent curve of BTL-I, BTL-MK and ketotifen.

hexosaminidase release was used as an index of degranulation. As shown in Figure 2A, among the tested compounds, BTL-I (**1**), **7**, and BTL-MK (**19**) showed strong degranulation inhibitory activity with inhibition rates exceeding 90%, which were superior to that of the positive inhibitor (Ketotifen). Additionally, the inhibitory activity of BTL-I was weakened to varying degrees when its hydroxyl group was modified by alkylation or acylation, indicating that the hydroxyl group of BTL-I plays an important role in maintaining its inhibitory activity. It is noteworthy that the methyl carboxylate group of BTL-I was reduced to an alcohol (**17**), and its inhibitory activity was significantly reduced. However, the inhibitory activity increased 2-fold after oxidation to an aldehyde (**18**) and further increased after conversion to a methyl ketone (**19**), which surpassed the lead compound BTL-I. These results indicated that the carbonyl group was a necessary functional group for BTL-I to exert its pharmacological activity. Taking into account the fact that the methyl ester group of compound **7** may be rapidly metabolized by carboxylesterase, we decided to conduct a more comprehensive investigation of BTL-MK. As shown in Figure 2B, the dose-inhibition assay demonstrated that BTL-MK could effectively inhibit the degranulation of mast cells in a dose-dependent manner, with an IC_{50} value of 6.7 μM, which was significantly lower than that of BTL-I (13.5 μM) and ketotifen (27.9 μM). Noteworthily, BTL-MK exhibited no significant cytotoxicity against RBL-2H3 cells, even at a concentration of up to 100 μM (Figure S37). These results indicated that BTL-MK may be potentially developed as an orally bioavailable antiallergic agent with excellent degranulation inhibitory activity and good pharmacokinetic properties.

***In Vivo* Antiallergic Activities of BTL-MK.** To investigate the antiallergic activity of BTL-MK *in vivo*, an ovalbumin (OVA)-induced food allergy mice model was established.[29,30] The protocol of the murine model was shown in Figure 3A, where OVA-sensitized mice were administered BTL-MK (2.5, 5.0, and 10 mg/kg) once a day during the OVA challenge phase (days 28−40) by gavage. The spleen is the largest lymphatic organ of the body and functions as the immune response. When an abnormal immune response occurs, spleen enlargement will be caused. Figure 3B shows a direct view of the spleen size of mice in different groups. Compared to the phosphate-buffered saline (PBS) group, the spleen of mice in the OVA group was significantly enlarged, indicating that OVA-induced food allergy in this model caused abnormal immune responses in mice. While compared to the OVA group, the spleen of the mice in the BTL-MK group was significantly smaller, suggesting that the allergic response of the mice to OVA was suppressed after the intervention of BTL-MK. OVA protein is digested and degraded in the gastrointestinal tract after oral ingestion, and abnormal immune response caused by allergy will lead to intestinal barrier damage, manifested as intestinal edema, diarrhea, and microbial imbalance. As can be seen from Figure 3C, compared with the PBS group, the intestinal tract of mice in the OVA group was significantly edema and the intestinal cavity contents were shapeless, indicating that the intestinal tract of mice in the OVA group was damaged due to allergic reaction. However, compared with the OVA group, the intestinal tract of mice in the BTL-MK group did not show edema, and the intestinal cavity contents were granular, indicating that the intestinal barrier damage of mice was alleviated after BTL-MK intervention. As shown in Figure 3D−F, the serum IgE, IgG1, and IgG2a levels were increased robustly in response to OVA. In contrast, treatment with BTL-MK significantly decreased the levels of OVA-specific IgE and IgG1 in a dose-dependent manner at concentrations of 2.5, 5.0, and 10 mg/kg. In contrast, the serum levels of IgG2a (Th1-related Ig) were not reversed by the BTL-MK administration. Histamine and mMCP-1 were the important mediators of mast cells, which were significantly elevated in the serum of OVA-induced mice and significantly decreased by BTL-MK treatment, and which were almost equivalent to those of the PBS control group (Figure 3G,H). Similarly, Th2-related cytokine IL-4 was observed to increase food allergy and was also significantly suppressed by BTL-MK treatment (Figure 3I). Furthermore, IFN-γ as a Th1-related cytokine was decreased in the OVA-induced group and was reversed considerably by BTL-MK administration at 10 mg/kg (Figure 3J).

Because of their speed and convenience, passive cutaneous anaphylaxis (PCA) models are often used to study the effects of antiallergy drugs on mouse mast cells. In the PCA model (Figure 4A), venous blood carries bovine serum albumin (BSA) throughout the body. BSA binds to IgE in the ear of mice, causing mast cell degranulation, enhancing vascular permeability, and thus causing extravasation of Evans blue dye. So, the depth and size of the blue patches on a mouse's ear can be used to measure the severity of an allergic reaction. As shown in Figure 4B, compared to the PBS group, blue plaques were visible in the ears of mice in the 2,4-dinitrophenylated bovine serum albumin (DNP-BSA) group, indicating that the

https://doi.org/10.1021/acs.jmedchem.4c00354
J. Med. Chem. 2024, 67, 7504−7515

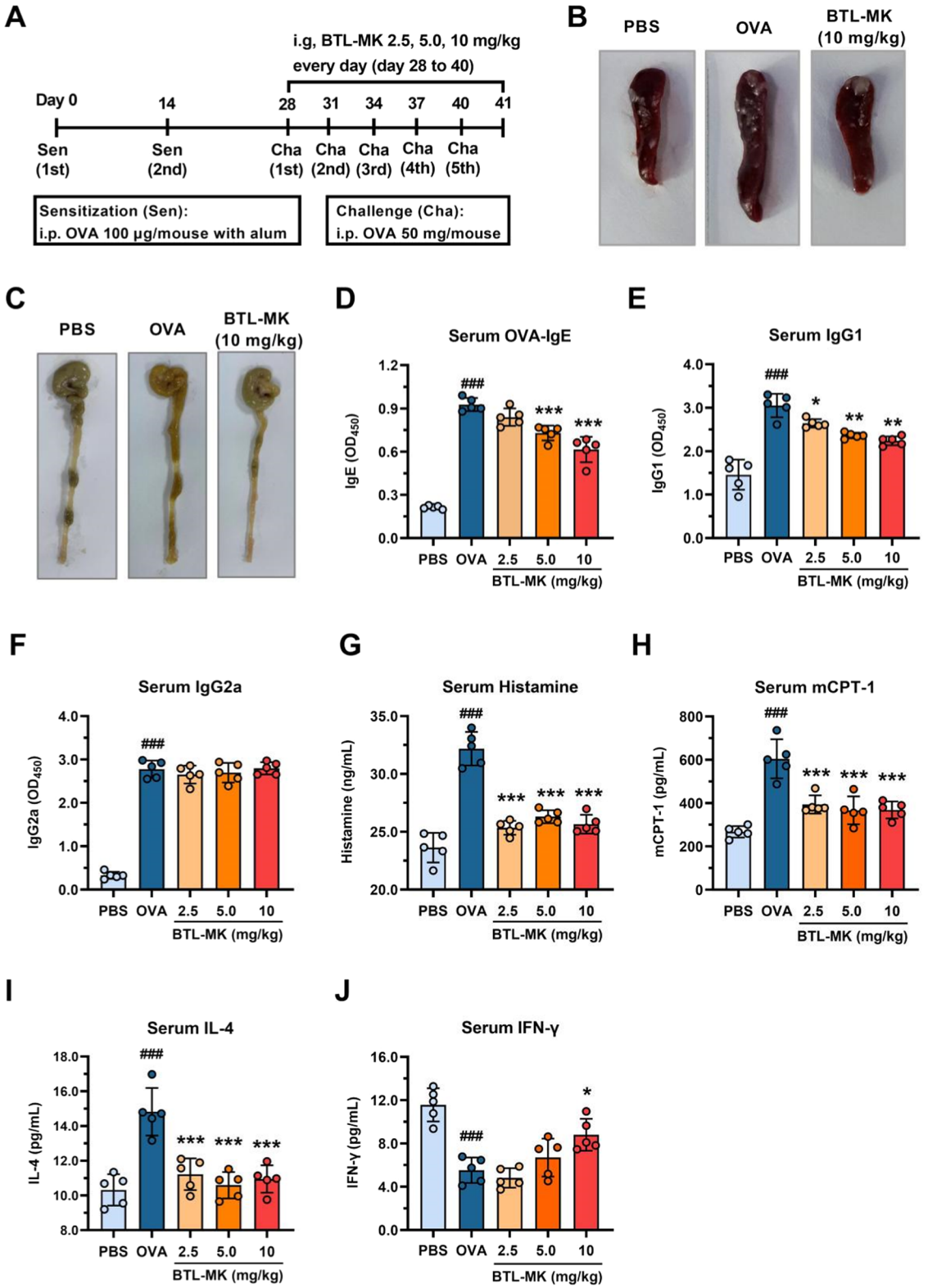

Figure 3. Effects of BTL-MK on the allergic response in the OVA-induced mice model. (A) Experimental time scheme. (B, C) Macroscopic view of a representative spleen and large intestine from each group of mice. (D) Effect of BTL-MK on the OVA-specific IgE. (E) Effect of BTL-MK on OVA-specific IgG1. (F) Effect of BTL-MK on OVA-specific IgG2. (G) Effect of BTL-MK on histamine release. (H) Effect of BTL-MK on mMCP-1 release. (I) Effect of BTL-MK on cytokine IL-4 release. (J) Effect of BTL-MK on IFN-γ release. Statistical differences are indicated by P values (one-way analysis of variance (ANOVA)), $^{*}P < 0.05$, $^{**}P < 0.01$, $^{***}P < 0.001$ *vs* OVA group. $^{\#\#\#}P < 0.001$ *vs* PBS group.

model was successfully constructed. The intervention of BTL-MK inhibited Evans blue extravasation in the ear of mice. In addition, with the increase of BTL-MK concentration, the blue depth steadily decreased, indicating that the inhibition of BTL-MK on the ear of mice was concentration-dependent. The quantitative study of blue dye infiltration inside and outside the

https://doi.org/10.1021/acs.jmedchem.4c00354
J. Med. Chem. 2024, 67, 7504−7515

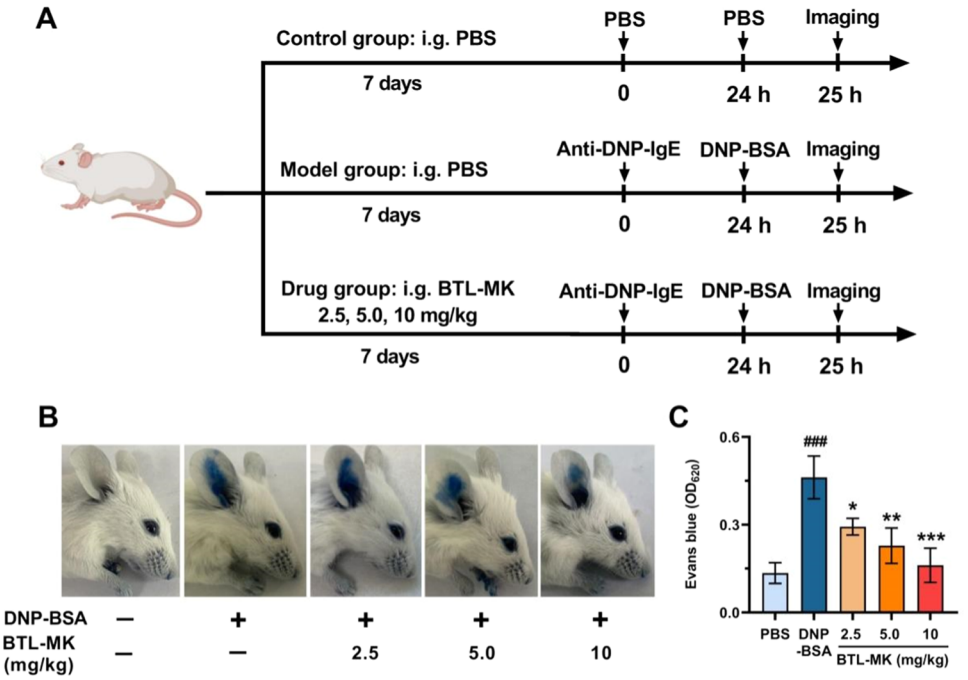

Figure 4. Effects of BTL-MK on the mice PCA reaction. (A) Experimental time scheme. (B) Macroscopic view of a representative mice ear from each group. (C) Allergic reaction was assessed by measuring the extravasation of Evans blue dye. Statistical differences are indicated by *P* values (one-way ANOVA), $^{*}P < 0.05$, $^{**}P < 0.01$, $^{***}P < 0.001$ *vs* DNP-BSA group. $^{\#\#\#}P < 0.001$ *vs* PBS group.

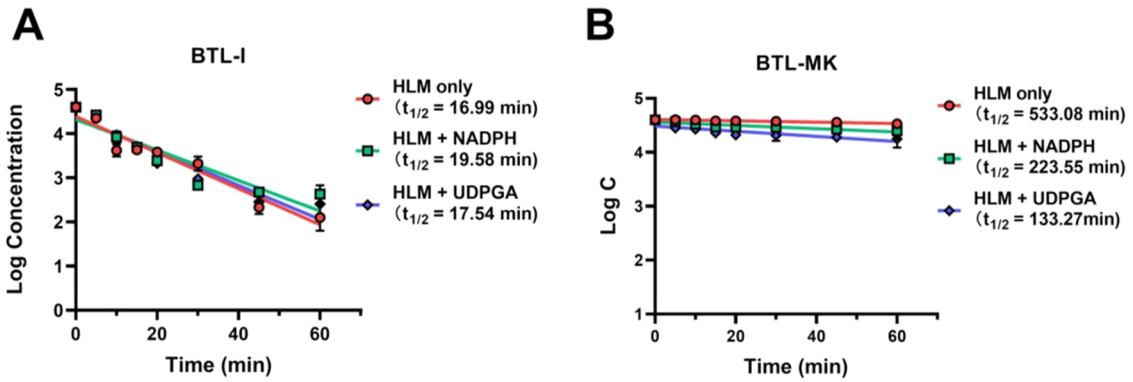

Figure 5. Metabolic half-lives of BTL-I (A) and BTL-MK (B) in HLM.

ears of mice is shown in Figure 4C. The dye level in the ears of mice in the 2,4-dinitrophenylated bovine serum albumin (DNP-BSA) group was significantly higher than that in the PBS group. In contrast, blue dyes were significantly reduced in a concentration-dependent manner after intervention with different concentrations of BTL-MK compared with the DNP-BSA group. These results suggest that BTL-MK can inhibit mast cell degranulation in mice.

***In Vitro* Metabolic Stability of BTL-MK.** The poor metabolic stability of BTL-I is a significant limitation in terms of its pharmacokinetic properties. It was observed that the methyl ester group of BTL-I is crucial for its rapid metabolism, which was confirmed through *in vitro* metabolic profiles and similar metabolic half-lives in human liver microsomes (HLM) with different enzymatic cofactors (Figure 5A).[31−34] The $t_{1/2}$ of BTL-I in HLM with nicotinamide adenine dinucleotide phosphate (NADPH) and uridine diphosphate glucuronic acid (UDPGA) were 19.58 and 17.54 min, respectively, similar to that in HLM without cofactors ($t_{1/2}$ = 16.99 min). These findings suggest that the methyl ester moiety of BTL-1 serves as the primary metabolic site for carboxylesterases, with BTL-1 primarily cleared through esterase metabolism, while metabolism by cytopigments (CYPs) and UGTs is minimal. As expected, the substitution of the carboxylic ester group with a methyl ketone group (BTL-MK) significantly improved its metabolic stability in HLM without affecting its antiallergic activity. Under various enzymatic cofactor reaction conditions, BTL-MK was found to be hardly metabolized in HLM, with metabolic half-lives of 533.08, 223.55, and 133.27 min (Figure 5B). These results demonstrated that BTL-MK has significantly enhanced *in vitro* metabolic stability, making it a potential candidate as an oral antiallergic agent compared to BTL-I.

Pharmacokinetics of BTL-MK by Oral and Intravenous Administration *In Vivo*. Having evaluated the effect of BTL-MK on the antiallergic activity and microsomal stability, the *in vivo* pharmacokinetics of BTL-MK were further investigated after intravenous (iv, 10 mg/kg, $n = 6$) and oral administration (po, 40 mg/kg, $n = 6$) in rats to demonstrate its suitability for extensive *in vivo*. As shown in Table 1, a

https://doi.org/10.1021/acs.jmedchem.4c00354
J. Med. Chem. 2024, 67, 7504−7515

Table 1. Key Pharmacokinetic Parameters of BTL-I and BTL-MK in Rats

	BTL-I		BTL-MK	
parameters	iv (10 mg/kg)	po (40 mg/kg)	iv (10 mg/kg)	po (40 mg/kg)
T_{max} (h)		0.7 ± 0.2		0.2 ± 0.06
C_{max} (μg/L)		10.8 ± 2.7		6105.6 ± 1157.0
AUC_{0-12h} (μg/(L·h))	21.7 ± 7.4	28.9 ± 4.3	4088.2 ± 1263.4	6536.9 ± 799.3
$AUC_{0-\infty}$ (μg/(L·h))	27.8 ± 12.0	36.9 ± 12.3	4119.2 ± 1252.4	7558.9 ± 1225.9
CL (L/h/kg)	432.1 ± 209.3	1082.2 ± 274.2	2.7 ± 0.9	5.4 ± 1.0
$T_{1/2}$ (h)	4.1 ± 3.3	4.7 ± 2.7	2.2 ± 0.6	4.1 ± 1.5
F (%)		33.2		45.9

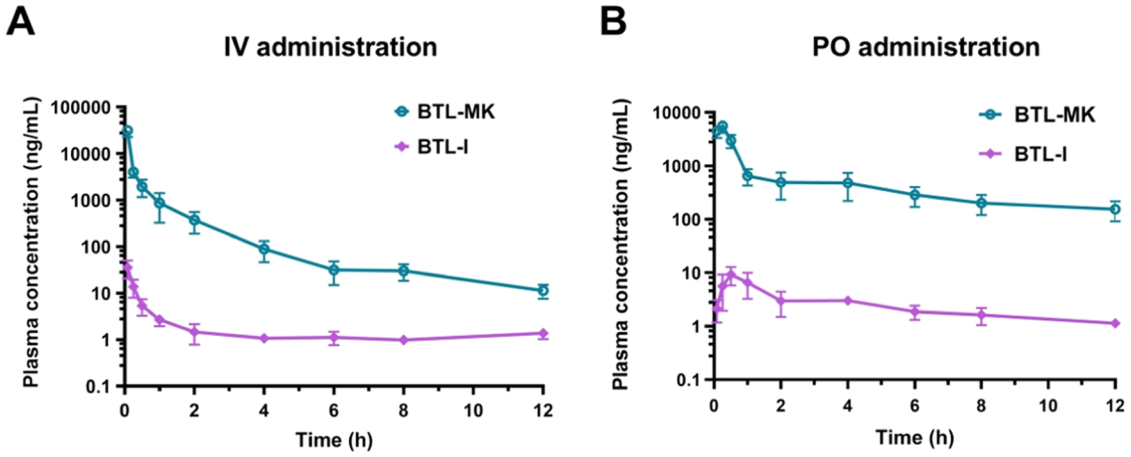

Figure 6. Drug concentration−time curves of BTL-I and BTL-MK by intravenous administration (A) and oral administration (B).

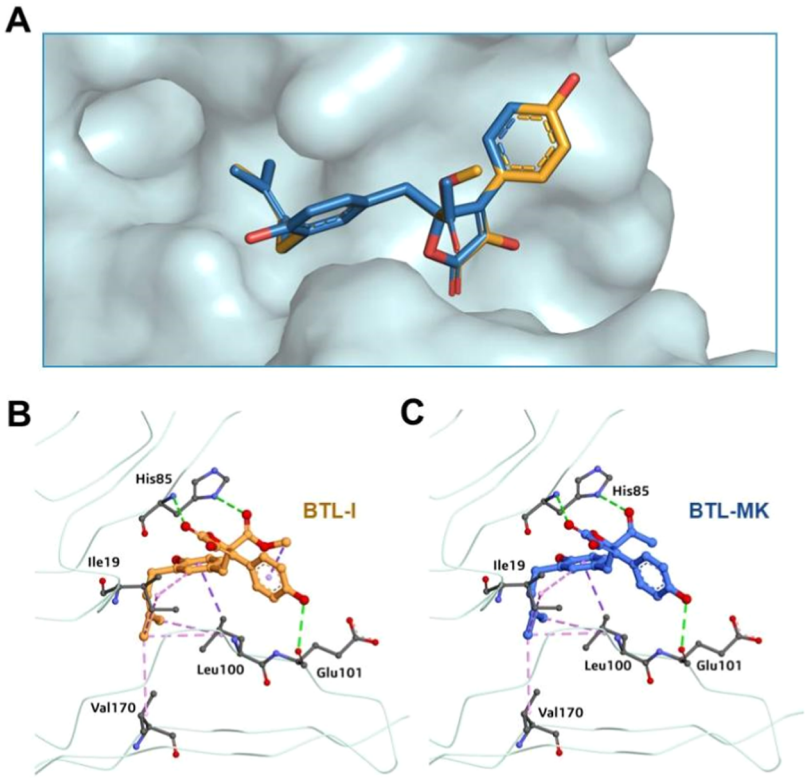

Figure 7. Three-dimensional (3D) receptor−ligand interaction analysis. (A) BTL-I (orange) and BTL-MK (blue) bound to FcγRIIB (PDB Code: 2fcb) in highly overlapped way. (B, C) Docking poses of BTL-I (orange) and BTL-MK (blue) docked to FcγRIIB. The protein structure of FcγRIIB was shown in cartoon type with the transparent surface colored light green. In the partially enlarged images (B, C), protein structures were shown in light green tubes. van der Waals were light green. Conventional hydrogen bonds were green. $\pi-\sigma$ was shown in purple. Alkyl and π-alkyl were shown in pink.

https://doi.org/10.1021/acs.jmedchem.4c00354
J. Med. Chem. 2024, 67, 7504−7515

significant decline in the total clearance (from 432.1 to 2.7 L/h/kg) and a significantly shortened elimination half-life (from 4.1 to 2.2 h) of BTL-MK were found, resulting in a remarkable increase in the area under the curve (AUC) value of BTL-MK (from 27.8 to 4119.2 g/(L·h)), compared with BTL-I. In general, a lower clearance rate was accompanied by an increase in oral exposure, which may be due to lower first-pass metabolism. Compared with BTL-I, the clearance rate of BTL-MK was lower than that of 1% of BTL-I. Meanwhile, a comparative analysis of pharmacokinetic parameters for BTL-I and BTL-MK after oral administration was also conducted. The methyl ketone substituent leads to a significant increase in the exposure to BTL-MK. The oral C_{max} value (6105.6 μg/L) of BTL-MK was remarkably higher than that of BTL-I (10.8 μg/L). The methyl ketone substituent also caused a huge increase in the oral AUC value (from 36.9 to 7558.9 μg/(L·h)) and a remarkable decrease in clearance (from 1082.2 to 5.4 L/h/kg) of BTL-MK, compared with BTL-I. More importantly, the absolute oral bioavailability (F) of BTL-MK was determined to be 45.9%, and it showed sufficient plasma concentrations in rats (Figure 6). Taken together, these results strongly suggested that the metabolic stability of BTL-MK was significantly improved while its first-pass effect was decreased considerably, making it a good candidate for the treatment of FAs and following proof-of-principle study.

BTL-MK Binds to the Inhibitory Receptor FcγRIIB. The molecular docking simulations were conducted to analyze the binding mechanisms of BTL-I derivatives against FcγRIIB.[35,36] As shown in Figure 7 and Table S5, BTL-I and BTL-MK bound to FcγRIIB in a highly overlapped way, and the interacting residues of the two inhibitors were the same. BTL-I and BTL-MK formed two hydrogen bonds with His85, one hydrogen bond with Glu101, a $\pi-\sigma$ interaction with Leu100, and other hydrophobic interactions (alkyl and π-alkyl) with Ile19 as well as Val 170. Furthermore, the molecular docking simulation results of all BTL-I derivatives indicated a moderate correlation between predicted binding energies and antiallergic activities of compounds (Table S5). According to the predicted binding energy calculated by Vina, BTL-I was less compatible with FcγRIIB than BTL-MK. BTL-I bound to FcγRIIB with a value of −7.131 kcal/mol. BTL-MK bound to FcγRIIB with the value of −7.418 kcal/mol. The observation suggests that BTL-I and BTL-MK are firmly bound to FcγRIIB, and BTL-MK should form a more stable receptor−ligand complex with FcγRIIB.

CONCLUSIONS

In summary, we have successfully mitigated the challenge of metabolic instability and antiallergic activity associated with lead compound BTL-I. The methyl carboxylate group of BTL-I is the key group that leads to its rapid metabolic clearance by carboxylesterases, and the carbonyl group of the methyl carboxylate group plays an important role in maintaining its antiallergic activity. Thus, the methyl carboxylate group of BTL-I was replaced by methyl ketone to form BTL-MK, which displayed a 2-fold improvement in activity *in vitro*, and more importantly, C_{max} (po) and $AUC_{0-\infty}$ (po) are increased by 565 and 204 times, respectively, compared to BTL-I. BTL-MK exhibited potent antiallergic activity *in vitro* and *in vivo* along with favorable oral exposure and a high oral bioavailability in rats, suggesting that it has the potential to deliver a drug candidate for the treatment of FAs, and these findings provide helpful guidance for druggability optimization of lead compounds.

EXPERIMENTAL SECTION

Synthetic Material and Equipment. Unless otherwise stated, all reactions were carried out under an argon atmosphere with dry solvents under anhydrous conditions. Unless otherwise stated, all of the chemicals were purchased commercially and used without further purification. The boiling point of petroleum ether (PE) is between 60−90 °C. Tetrahydrofuran (THF) was distilled from sodium-benzophenone; *n*-hexane was distilled from sodium under argon atmosphere; dichloromethane (CH_2Cl_2) and diethyl ether were distilled from calcium hydride under argon atmosphere. Toluene was distilled from sodium under argon atmosphere. Superdry MeOH was purchased from Innochem Science & Technology Co., Ltd. Reactions were monitored by thin layer chromatography (TLC) carried out on 0.25 mm Qingdao silica gel plates (60F-254) using UV lights as the visualizing agent and $KMnO_4$. Flash column chromatography was performed over Qingdao silica gel (200−300 mesh). Infrared spectra were recorded on a Nicolet AVATAR FTIR380 spectrometer as a thin film and were reported in reciprocal centimeters (cm^{-1}). High-resolution mass spectra (HRMS) were recorded on a Micromass QTOF2 Quadrupole/Time-of-Flight Tandem mass spectrometer using electron spray ionization. NMR spectra were recorded on Bruker AV-400, Bruker AV-500, and Bruker AV-600 instruments and were calibrated using residual undeuterated solvents ($CHCl_3$, δ_H = 7.26) and deuterated solvents ($CDCl_3$, δ_C = 77.0) as internal references. The data for ^1H NMR are reported as follows: chemical shift, multiplicity (s = singlet, d = doublet, t = triplet, m = multiplet or unresolved, brs = broad singlet), coupling constants (Hz), and integration. All compounds are >95% pure by high-performance liquid chromatography (HPLC) analysis.

Synthesis of the Hydroxyl Group-Modified Derivatives. To a solution of **1** (349.0 mg, 0.825 mmol) in acetonitrile (10 mL) was added potassium carbonate (690.0 mg, 5.0 mmol), and the mixture was stirred for half an hour. Then, methyl iodide (218.0 mg, 1.55 mmol) was added, and the reaction mixture was stirred for 1 h before the addition of saturated NH_4Cl. The mixture was extracted with EtOAc (3 × 100 mL). The combined organic layer was washed with brine, dried over $MgSO_4$, and concentrated *in vacuo*. Purification of the residue by flash chromatography (PE/EtOAc = 20:1−1:1) afforded methyl-substituted derivatives **2** (62.0 mg, yield 18%), **3** (110.6 mg, yield 32%), and **4** (65.7 mg, yield 19%).

To a solution of **1** (250.0 mg, 0.47 mmol) in acetone (20 mL) was added potassium carbonate solid (489.0 mg, 3.54 mmol), and the mixture was stirred for half an hour. Then, allyl bromide (143.0 mg, 1.18 mmol) was added, and the reaction mixture was stirred for 2 h before the addition of saturated NH_4Cl. The mixture was extracted with EtOAc (3 × 100 mL). The combined organic layer was washed with brine, dried over $MgSO_4$, and concentrated *in vacuo*. Purification of the residue by flash chromatography (PE/EtOAc = 25:1−4:1) afforded allyl-substituted derivatives **5** (30.2 mg, yield 9%), **6** (183.7 mg, yield 62%), and **7** (39.7 mg, yield 15%).

To a solution of **1** (500 mg, 1.2 mmol) in acetone (20 mL) was added potassium carbonate solid (1.5 g, 10.8 mmol), and the mixture was stirred for half an hour. Then, 1-bromo-3-methyl-2-butene (0.5 g, 3.6 mmol) was added, and the reaction mixture was stirred for 2 h before the addition of saturated NH_4Cl. The mixture was extracted with EtOAc (3 × 100 mL). The combined organic layer was washed with brine, dried over $MgSO_4$, and concentrated *in vacuo*. Purification of the residue by flash chromatography (PE/EtOAc = 40:1) afforded 1-bromo-3-methyl-2-butenyl-substituted derivatives **8** (428 mg, yield 57%).

To a solution of **1** (117.5 mg, 0.28 mmol) in dichloromethane (10 mL) was added triethylamine (85.0 mg, 0.84 mmol), and the mixture was stirred for half an hour. Then, acetyl chloride (65.5 mg, 0.84 mmol) was added, and the reaction mixture was stirred for 1 h before the addition of saturated NH_4Cl. The mixture was extracted with EtOAc (3 × 100 mL). The combined organic layer was washed with

https://doi.org/10.1021/acs.jmedchem.4c00354
J. Med. Chem. 2024, 67, 7504−7515

brine, dried over $MgSO_4$, and concentrated *in vacuo*. Purification of the residue by flash chromatography (PE/EtOAc = 20:1−1:1) afforded acetyl-substituted derivatives **9** (23.2 mg, yield 15%), **10** (19.1 mg, yield 13%), and **11** (4.6 mg, yield 2%).

To a solution of **1** (695.1 mg, 1.64 mmol) in dichloromethane (40 mL) was added triethylamine (663.9 mg, 6.56 mmol), and the mixture was stirred for half an hour. Then, 2-methylpropionyl chloride (143.0 mg, 1.18 mmol) was added, and the reaction mixture was stirred for 1 h before the addition of saturated NH_4Cl. The mixture was extracted with EtOAc (3 × 100 mL). The combined organic layer was washed with brine, dried over $MgSO_4$, and concentrated *in vacuo*. Purification of the residue by flash chromatography (PE/EtOAc = 20:1−1:1) afforded dimethylpropyl-substituted derivatives **12** (130.6 mg, yield 13%), **13** (101.9 mg, yield 11%), and **14** (5.2 mg, yield 1%).

Synthesis of Neopentyl Group-Modified Derivatives 15 and 16. To a solution of **1** (30.0 mg, 0.07 mmol) in MeOH (10 mL) was added palladium on carbon (4.3 mg, 0.04 mmol) under an argon atmosphere and then evacuated with argon three times, and then the hydrogen balloon was connected to the reaction flask. Then, silica gel was added, and the mixture was concentrated *in vacuo*. Purification of the residue by flash chromatography (CH_2Cl_2/CH_3OH = 100:3) afforded a reduction derivative in neophenyl group **15** (20.4 mg, yield 68%).

To a solution of **1** (90.2 mg, 0.21 mmol) in MeOH (10 mL) was added HCl solution (0.1 mL, 1.0 mol/L), and the mixture was stirred for 12 h. Then, saturated sodium bicarbonate solution was added and stirred for 0.5 h. The mixture was extracted with EtOAc (3 × 100 mL). The combined organic layer was washed with brine, dried over $MgSO_4$, and concentrated *in vacuo*. Purification of the residue by flash chromatography (CH_2Cl_2/CH_3OH = 100:1) afforded cyclization of neophenyl group derivative **16** (58.6 mg, yield 66%).

Synthesis of Ester Group-Modified Derivatives. To a solution of **1** (4.17 g, 9.8 mmol) in dichloromethane (20 mL) was added imidazole (2.67 g, 39.3 mmol) and stirred for 0.5 h. Then, TBSCl (5.9 g, 39.3 mmol) was added and stirred for 4 h before the addition of saturated ammonium chloride solution. The mixture was extracted with EtOAc (3 × 100 mL). The combined organic layer was washed with brine, dried over $MgSO_4$, and concentrated *in vacuo*. Purification of the residue by flash chromatography (PE/EtOAc = 40:1) afforded TBS-protected butyrolactone I (**20**, 5.6 g, yield 74%).

To a solution of **20** (431.3 mg, 0.56 mmol) in ultradry MeOH (20 mL) was added lithium borohydride in tetrahydrofuran (0.56 mL, 1.13 mmol). The mixture was stirred for 4 h before the addition of saturated ammonium chloride solution. The mixture was extracted with EtOAc (3 × 100 mL). The combined organic layer was washed with brine, dried over $MgSO_4$, and concentrated *in vacuo*. Purification of the residue by flash chromatography (PE/EtOAc = 20:1) afforded a TBS-protected primary alcohol derivative of butyrolactone I (**21**, 296.1 mg, yield 74%).

To a solution of **21** (170 mg, 0.23 mmol) in tetrahydrofuran (20 mL) was added tetra-*n*-butylammonium fluoride (0.56 mL, 1 mol/L in tetrahydrofuran). The mixture was stirred for 0.5 h before the addition of saturated ammonium chloride solution. The mixture was extracted with EtOAc (3 × 100 mL). The combined organic layer was washed with brine, dried over $MgSO_4$, and concentrated *in vacuo*. Purification of the residue by flash chromatography (CH_2Cl_2/CH_3OH = 100:3) afforded the primary alcohol derivative of butyrolactone I (**17**, 83.6 mg, yield 92%).

To a solution of **21** (120 mg, 0.16 mmol) in dichloromethane (2 mL) was added Dess−Martin oxidant (136 mg, 0.32 mmol). The mixture was stirred for 0.5 h before the addition of saturated sodium sulfite solution and sodium bicarbonate solution. The mixture was extracted with dichloromethane (3 × 2 mL). The combined organic layer was washed with brine, dried over $MgSO_4$, and concentrated *in vacuo*. Purification of the residue by flash chromatography (PE/EtOAc = 20:1) afforded the TBS-protected aldehyde derivative of butyrolactone I (**22**, 68 mg, yield 57%).

To a solution of **22** (97.3 mg, 0.13 mmol) in tetrahydrofuran (20 mL), tetra-*n*-butylammonium fluoride (0.65 mL,1 mol/L in tetrahydrofuran) was added. The mixture was stirred for 0.5 h before the addition of saturated ammonium chloride solution. The mixture was extracted with EtOAc (3 × 100 mL). The combined organic layer was washed with brine, dried over $MgSO_4$, and concentrated *in vacuo*. Purification of the residue by flash chromatography (CH_2Cl_2/CH_3OH = 100:3) afforded the primary aldehyde derivative of butyrolactone I (**18**, 83.6 mg, yield 92%).

To a solution of **22** (40.0 mg, 0.05 mmol) in dichloromethane (0.5 mL) was added dropwise a toluene solution of trimethylaluminum (0.04 mL, 1.6 mol/L). The mixture was stirred for 2 h at 25 °C before the addition of saturated ammonium chloride solution. The mixture was extracted with dichloromethane (3 × 2 mL). The combined organic layer was washed with brine, dried over $MgSO_4$, and concentrated *in vacuo*. The crude mixture was dissolved in dichloromethane (0.5 mL), and then Dess−Martin Reagent (68 mg, 0.16 mmol) was added. The mixture was stirred for 0.5 h before the addition of saturated sodium bicarbonate and saturated sodium sulfite. The mixture was extracted with dichloromethane (3 × 2 mL). The combined organic layer was washed with brine, dried over $MgSO_4$, and concentrated *in vacuo*. Purification of the residue by flash chromatography (PE/EtOAc = 40:1) afforded the TBS-protected methyl ketone derivative of butyrolactone I (**23**, 24 mg, yield 60%).

To a solution of **23** (92.5 mg, 0.12 mmol) in tetrahydrofuran (20 mL), tetra-*n*-butylammonium fluoride (0.6 mL, 1 mol/L in tetrahydrofuran) was added. The mixture was stirred for 0.5 h before the addition of saturated ammonium chloride solution. The mixture was extracted with EtOAc (3 × 100 mL). The combined organic layer was washed with brine, dried over $MgSO_4$, and concentrated *in vacuo*. Purification of the residue by flash chromatography (CH_2Cl_2/CH_3OH = 100:3) afforded the methyl ketone derivative of butyrolactone I (**19**, 40.2 mg, yield 80%).

Biological Materials. OVA, Evans blue, and antidinitrophenyl (DNP)-IgE were supplied by Sigma (St Louis, MO), and DNP-BSA was supplied by Biosearch (Petaluma, CA). Histamine and mouse mast cell proteinase (mMCP)-1 enzyme-linked immunosorbent assay (ELISA) kits were purchased from Jiangsu Meimian Industrial Co., Ltd. (Jiangsu, China). The antibodies for IgE, IgG1, and IgG2a were purchased from Abcam (Camb, U.K.). The mouse IL-4 and INF-γ kits were purchased from Neobioscience in Shenzhen, China.

***In Vitro* Antiallergic Activity.** RBL-2H3 cells were cultured in a 96-well plate with 2 × 10^5 cells/well, incubated with anti-DNP-IgE (200 ng/mL). After 16 h, cells were washed with PBS. Then, a benchtop solution was added, followed by stimulation with DNP-BSA. After incubation, the cells were lysed, and the cell lysate was collected. Those test solutions are used to test the efficiency of degranulation, mainly detecting the release of β-aminosidase. We apply the following formula to calculate the inhibition rate of the sample to be tested for cell degranulation (the sample is added to the system 1 h before the DNP-BSA stimulation) and calculate the inhibition rate by comparing and calculating the degranulation efficiency of different groups

$$=100\% \times (\text{DNP-BSA group} - \text{sample group}) / (\text{DNP-BSA group} - \text{PBS group}) \quad (1)$$

OVA-Induced Mouse Food Allergy Model. BALB/c female mice were purchased from Shanghai Laboratory Animal Center, Chinese Academy of Sciences, aged 6−8 weeks and weighing 20 ± 2 g. The mice were placed in a specific pathogen-free (SPF) environment, light/dark cycle for 12 h, stable temperature of 22 ± 1 °C, relative humidity of 55 ± 10%, and a free diet. All programs are authorized by the Jimei University Animal Research Ethics Committee (Xiamen, China; SCXK 2016-0006).

The animal model was constructed according to the reported methods.[37,38] OVA was used as the sensitizer (combined with alum) to sensitize Balb/c mice, and the detailed immunization regimen is shown in Figure 3A. On days 0 and 14, each mouse was sensitized by intraperitoneal injection of an OVA/alum mixture, and the OVA/aluminum adjuvant was 1:1 (OVA content was 5 mg/kg, PBS was used instead of OVA in the PBS group). The mice were randomly divided into five mice per group: PBS group, OVA group, and BTL-

https://doi.org/10.1021/acs.jmedchem.4c00354
J. Med. Chem. 2024, 67, 7504−7515

MK group with different concentrations. According to the experimental protocol, different doses of drugs were injected into the stomach every day from the 28th day. From the 28th day, OVA (50 mg/mouse) was given to the mice by intragastric administration (the PBS group was given intragastric administration with PBS), which was stimulated every 2 days. After the fifth gavage, serum was collected from the tail vein of mice within 1 h, and blood was collected from the eyeball the next day. The serum was stored at −80 °C for later use. The mice were killed, and the spleen and intestines were dissected and photographed.

PCA Model. The passive cutaneous anaphylaxis (PCA) mouse model was constructed according to the previous method.[39] A total of 25 BALB/c female mice weighing 20 ± 2 g were randomly divided into five groups. In the PBS and DNP-BSA groups, anti-DNP-IgE (5 μg/mL, 100 μL) was injected intradermically into the left ear of each mouse. After 24 h, 100 μL of DNP-BSA was injected intravenously (10 mg/mL Evans blue solution plus 2 mg/mL DNP-BSA), while BTL-MK (2.5, 5, 10 mg/kg) was administered *via* gavage for 7 days prior to the injection of anti-DNP-IgE and the subsequent administration of DNP-BSA in the BTL-MK group. Subsequently, the mice were granted 1 h of unrestricted movement, after which they were gently sedated, and photographs of their left ears were taken. After photographing, the mice were euthanized, and the left ear was taken, cut into pieces, mixed with 3 M KOH, and incubated at 37 °C for 12 h. Acetone and phosphoric acid were mixed at a 13:5 ratio and added into the KOH system for a neutralization reaction. After centrifugation, the supernatant was taken, and absorbance was determined at 620 nm to quantify the dye content in mouse ears.

***In Vitro* Metabolic Stability.** *UGT Metabolic Stability Study.* The total reaction volume was 200 μL, which contained 20 mg/mL human liver microsomes (HLM), 50 mM Tris−HCl buffer (pH 7.4), 5 mM $MgCl_2$, and 0.5 mg/mg of protein Brij58. Then, 1 μL of substrate (BTL-I and BTL-MK, 2 mM in dimethyl sulfoxide (DMSO)) was added to the reaction mixture. After a 3 min preincubation, 10 μL of UDPGA was added to initiate the reaction. At 0, 5, 10, 15, 20, 30, 45, and 60 min, 100 μL of acetonitrile was added to terminate the reaction. The reaction mixture was centrifuged at 20,000*g* and 4 °C for 20 min, and 150 μL of the supernatant was analyzed by HPLC.

CYP Metabolic Stability Study. The total reaction volume was 200 μL, which contained 20 mg/mL human liver microsomes (HLM), 100 mM potassium phosphate buffer (pH 7.4), 40 mM $MgCl_2$, 100 mM glucose-6-phosphate (G-6-P), and 1 μL of substrate (BTL-I and BTL-MK, 2 mM in DMSO). After a 3 min preincubation, 20 μL of NADP was added to initiate the reaction. At 0, 5, 10, 15, 20, 30, 45, and 60 min, 100 μL of acetonitrile was added to terminate the reaction. The reaction mixture was centrifuged at 20,000*g* and 4 °C for 20 min, and 150 μL of the supernatant was analyzed by HPLC.

***In Vivo* Pharmacokinetic Study.** Twelve Sprague-Dawley (SD) rats, males weighing 180−220 g, were randomly divided into two groups and fasted for 12 h before the test, with free access to water. The food was uniformly fed for 2 h after drug administration. BTL-I and BTL-MK were dissolved in 5% dimethyl sulfoxide, 5% Tween-80, and 90% saline. Animals were subjected to an intravenous injection of 10 mg/kg and a gavage administration of 40 mg/kg, respectively. The time of administration was recorded, and 100 μL of venous blood was sampled from the jugular vein of rats at time points of 0.083, 0.25, 0.5, 1, 2, 4, 6, 8, and 12 h and placed in heparinized test tubes. The plasma sample was harvested by centrifuging blood at 4000*g* for 10 min immediately after sampling and then stored at −20 °C until further preparation.

Mass spectrometry conditions were used to quantify BTL-I in plasma in negative ion mode. BTL-I showed the parent ion $[M - H]^-$ at m/z 423.1 and the parent cation $[M - H]^-$ at m/z 845.6 for IS. In the production scanning mode, BTL-I and BTL-MK showed product ions at m/z 364.1 and 799.5, respectively. Therefore, m/z 423.1−364.1 was used for BTL-I and m/z 845.6−799.5 for BTL-MK as MRM transitions. An aqueous solution of acetonitrile and 0.1% FA was chosen as the mobile phase.

Docking Simulations. Docking of BTLs to FcγRIIB was conducted using AutoDockTools 1.5.7, with subsequent analysis performed using PyMOL software and DS Visualizer. The structures of BTLs were generated using Chem3D software (Cambridge Soft Co.) and then energy-minimized through steepest-descent and conjugate-gradient techniques. The crystal structure of human FcγRIIB was obtained from the Protein Data Bank (PDB Code: 2fcb) and was selected as a receptor. Prior to docking, all bound water and ligands were removed from the protein and polar hydrogens were added to the FcγRIIB model. Docking was performed using AutoDock Vina 1.2.3 with coordinates set at x = 23.236, y = 30.383, and z = 25.515. The grid box was sized as 15 $Å^3$, and a grid spacing of 0.375 Å was utilized. Following the completion of calculations, obtained conformations of FcγRIIB in complex with BTL-I were ranked based on binding energy, and docking graphics were generated using PyMOL software and DS Visualizer.

Statistical Analysis. The means ± standard deviations were utilized to present all results, with ANOVA employed to assess group differences. Pairwise comparisons were conducted using the Duncan highest significance difference test. Statistical significance was determined based on the following criteria: $*p < 0.05$, $**p < 0.01$, $***p < 0.001$, and $****p < 0.0001$. Three independent experiments involving mice were performed, with consistent results observed. The average values presented were derived from one of the three experiments, each group comprising five mice.

■ ASSOCIATED CONTENT

Supporting Information

The Supporting Information is available free of charge at https://pubs.acs.org/doi/10.1021/acs.jmedchem.4c00354.

NMR and MS data for compounds **2**−**23**, ^1H and ^{13}C NMR spectra for compounds **2**−**19**, cytotoxicity of BTL-I and butyrolactone methyl ketone (BTL-BK), HPLC traces for the lead compound BTL-BK, plasma concentration of BTL-I or BTL-BK at different time points after intravenous or oral administration, molecular docking simulations of BTL-I derivatives with FcγRIIB, as well as molecular formula strings and the antiallergic activities of BTL-I derivatives (PDF)

Molecular formula strings (CSV)

Binding modes of BTL-I derivatives with FcγRIIB (PDB code: 2fcb) (ZIP)

■ AUTHOR INFORMATION

Corresponding Authors

Xian-Wen Yang − *School of Pharmacy, Hainan Medical University, Hainan Academy of Medical Sciences, Haikou 571199, China; Key Laboratory of Marine Genetic Resources, Third Institute of Oceanography, Ministry of Natural Resources, Xiamen, Fujian 361005, China;* orcid.org/0000-0002-4967-0844; Phone: +86-592-2195319; Email: yangxianwen@tio.org.cn

Ping Wang − *Shanghai Frontiers Science Center of TCM Chemical Biology, Institute of Interdisciplinary Integrative Medicine Research, Shanghai University of Traditional Chinese Medicine, Shanghai 201203, China*; Phone: +86-21-51323180; Email: pwang@shutcm.edu.cn

Yandong Zhang − *State Key Laboratory of Physical Chemistry of Solid Surfaces, Key Laboratory of Chemical Biology of Fujian Province, iCHEM, College of Chemistry and Chemical Engineering, Xiamen University, Xiamen, Fujian 361005, China;* orcid.org/0000-0002-5558-9436; Phone: +86-592-2181851; Email: ydzhang@xmu.edu.cn

Guang-Ming Liu − *College of Ocean Food and Biological Engineering, Jimei University, Xiamen, Fujian 361021,*

https://doi.org/10.1021/acs.jmedchem.4c00354
J. Med. Chem. 2024, 67, 7504−7515

China; orcid.org/0000-0002-8689-0504;
Email: gmliu@jmu.edu.cn

Authors

Chun-Lan Xie − *School of Pharmacy, Hainan Medical University, Hainan Academy of Medical Sciences, Haikou 571199, China; Key Laboratory of Marine Genetic Resources, Third Institute of Oceanography, Ministry of Natural Resources, Xiamen, Fujian 361005, China*

Hong-Xiu Xiao − *Key Laboratory of Marine Genetic Resources, Third Institute of Oceanography, Ministry of Natural Resources, Xiamen, Fujian 361005, China; State Key Laboratory of Physical Chemistry of Solid Surfaces, Key Laboratory of Chemical Biology of Fujian Province, iCHEM, College of Chemistry and Chemical Engineering, Xiamen University, Xiamen, Fujian 361005, China*

Pei-Fang Song − *Shanghai Frontiers Science Center of TCM Chemical Biology, Institute of Interdisciplinary Integrative Medicine Research, Shanghai University of Traditional Chinese Medicine, Shanghai 201203, China*

Qing-Mei Liu − *College of Ocean Food and Biological Engineering, Jimei University, Xiamen, Fujian 361021, China*

Haoxiang Wei − *State Key Laboratory of Physical Chemistry of Solid Surfaces, Key Laboratory of Chemical Biology of Fujian Province, iCHEM, College of Chemistry and Chemical Engineering, Xiamen University, Xiamen, Fujian 361005, China*

Liang Wu − *Shanghai Frontiers Science Center of TCM Chemical Biology, Institute of Interdisciplinary Integrative Medicine Research, Shanghai University of Traditional Chinese Medicine, Shanghai 201203, China*

Guang-Hao Zhu − *Shanghai Frontiers Science Center of TCM Chemical Biology, Institute of Interdisciplinary Integrative Medicine Research, Shanghai University of Traditional Chinese Medicine, Shanghai 201203, China*

Complete contact information is available at:
https://pubs.acs.org/10.1021/acs.jmedchem.4c00354

Author Contributions

#C.-L.X., H.-X.X., P.-F.S., and Q.-M.L. contributed equally to this work.

Notes

The authors declare no competing financial interest.

ACKNOWLEDGMENTS

The work was financially supported by the National Key Research and Development Program of China (2022YFC2804205), the Xiamen Southern Oceanographic Center (22GYY007HJ07), and the National Natural Science Foundation of China (82274011, 22071205).

ABBREVIATIONS USED

$AUC_{0-\infty}$, area under the concentration−time curve; BTL-I, butyrolactone-I; BTL-BK, butyrolactone methyl ketone; C_{max}, maximum plasma concentration; CYP, cytopigment; DNP-BSA, 2,4-dinitrophenylated bovine serum albumin; FA, food allergy; FcγRIIB, Fc receptor IIB for IgG; FcεR1, Fc epsilon region receptor 1; MCs, mast cells; NADPH, nicotinamide adenine dinucleotide phosphate; OVA, ovalbumin; PCA, passive cutaneous anaphylaxis; PK, pharmacokinetic; UDPGA, uridine diphosphate glucuronic acid

REFERENCES

(1) Valenta, R.; Hochwallner, H.; Linhart, B.; Pahr, S. Food Allergies: The Basics. *Gastroenterology* **2015**, *148*, 1120.e4−1131.e4.
(2) Bieber, T. Disease Modification in Inflammatory Skin Disorders: Opportunities and Challenges. *Nat. Rev. Drug Discovery* **2023**, *22*, 662−680.
(3) Balz, K.; Kaushik, A.; Cemic, F.; Sampath, V.; Heger, V.; Renz, H.; Nadeau, K.; Skevaki, C. Cross-Reactive Mhc Class I T Cell Epitopes May Dictate Heterologous Immune Responses between Respiratory Viruses and Food Allergens. *Sci. Rep.* **2023**, *13*, No. 14874.
(4) Nowak-Wegrzyn, A.; Szajewska, H.; Lack, G. Food Allergy and the Gut. *Nat. Rev. Gastroenterol. Hepatol.* **2017**, *14*, 241−257.
(5) Anvari, S.; Miller, J.; Yeh, C. Y.; Davis, C. M. IgE-Mediated Food Allergy. *Clin. Rev. Allergy Immunol.* **2019**, *57*, 244−260.
(6) Guo, J.; Zhang, Y.; Liu, T.; Levy, B. D.; Libby, P.; Shi, G. P. Allergic Asthma Is a Risk Factor for Human Cardiovascular Diseases. *Nat. Cardiovasc. Res.* **2022**, *1*, 417−430.
(7) Florsheim, E. B.; Bachtel, N. D.; Cullen, J. L.; Lima, B. G. C.; Godazgar, M.; Carvalho, F.; Chatain, C. P.; Zimmer, M. R.; Zhang, C.; Gautier, G.; Launay, P.; Wang, A.; Dietrich, M. O.; Medzhitov, R. Immune Sensing of Food Allergens Promotes Avoidance Behaviour. *Nature* **2023**, *620*, 643−650.
(8) Tang, M. L. K.; Mullins, R. J. Food Allergy: Is Prevalence Increasing? *Intern. Med. J.* **2017**, *47*, 256−261.
(9) Seth, D.; Poowutikul, P.; Pansare, M.; Kamat, D. Food Allergy: A Review. *Pediatr. Ann.* **2020**, *49*, e50−e58.
(10) Krajewski, G. S.; Krajewski, T. Evaluation and Management of Food Allergies in the Emergency Department. *Emerg. Med. Clin. North Am.* **2022**, *40*, 57−67.
(11) Gupta, R. S.; Dyer, A. A.; Jain, N.; Greenhawt, M. J. Childhood Food Allergies: Current Diagnosis, Treatment, and Management Strategies. *Mayo Clin. Proc.* **2013**, *88*, 512−526.
(12) Epstein-Rigbi, N.; Levy, M. B.; Nachshon, L.; Koren, Y.; Katz, Y.; Goldberg, M. R.; Elizur, A. Efficacy and Safety of Food Allergy Oral Immunotherapy in Adults. *Allergy* **2023**, *78*, 803−811.
(13) Brar, K. K.; Lanser, B. J.; Schneider, A.; Nowak-Wegrzyn, A. Biologics for the Treatment of Food Allergies. *Immunol. Allergy Clin. North Am.* **2020**, *40*, 575−591.
(14) Pouessel, G.; Alonzo, S.; Divaret-Chauveau, A.; Dumond, P.; Bradatan, E.; Liabeuf, V.; Beaumont, P.; Tscheiller, S.; Diesnis, R.; Renaudin, J. M.; Sabouraud-Leclerc, D. Fatal and near-Fatal Anaphylaxis: The Allergy-Vigilance Network Data (2002−2020). *Allergy* **2023**, *78*, 1628−1638.
(15) Sicherer, S. H.; Sampson, H. A. Food Allergy: A Review and Update on Epidemiology, Pathogenesis, Diagnosis, Prevention, and Management. *J. Allergy Clin. Immunol.* **2018**, *141*, 41−58.
(16) Reber, L. L.; Marichal, T.; Mukai, K.; Kita, Y.; Tokuoka, S. M.; Roers, A.; Hartmann, K.; Karasuyama, H.; Nadeau, K. C.; Tsai, M.; Galli, S. J. Selective Ablation of Mast Cells or Basophils Reduces Peanut-Induced Anaphylaxis in Mice. *J. Allergy Clin. Immunol.* **2013**, *132*, 881−888.
(17) He, S. H.; Zhang, H. Y.; Zeng, X. N.; Chen, D.; Yang, P. C. Mast Cells and Basophils Are Essential for Allergies: Mechanisms of Allergic Inflammation and a Proposed Procedure for Diagnosis. *Acta Pharm. Sin. B* **2013**, *34*, 1270−1283.
(18) Rivera, J.; Gilfillan, A. Molecular Regulation of Mast Cell Activation. *J. Allergy Clin. Immunol.* **2006**, *117*, 1214−1225.
(19) St John, A. L.; Abraham, S. N. Innate Immunity and Its Regulation by Mast Cells. *J. Immunol.* **2013**, *190*, 4458−4463.
(20) Liu, Q. M.; Xie, C. L.; Gao, Y. Y.; Liu, B.; Lin, W. X.; Liu, H.; Cao, M. J.; Su, W. J.; Yang, X. W.; Liu, G. M. Deep-Sea-Derived Butyrolactone I Suppresses Ovalbumin-Induced Anaphylaxis by Regulating Mast Cell Function in a Murine Model. *J. Agric. Food Chem.* **2018**, *66*, 5581−5592.
(21) Bulfone-Paus, S.; Nilsson, G.; Draber, P.; Blank, U.; Levi-Schaffer, F. Positive and Negative Signals in Mast Cell Activation. *Trends Immunol.* **2017**, *38*, 657−667.

(22) Wu, L.; Xie, C. L.; Yang, X. W.; Chen, G. Pharmacokinetics and Metabolism Study of Deep-Sea-Derived Butyrolactone I in Rats by UHPLC−MS/MS and UHPLC−Q-TOF-MS. *Mar. Drugs* **2022**, *20*, 11.
(23) Wu, J.; Guan, X.; Dai, Z.; He, R.; Ding, X.; Yang, L.; Ge, G. Molecular Probes for Human Cytochrome P450 Enzymes: Recent Progress and Future Perspectives. *Coord. Chem. Rev.* **2021**, *427*, No. 213600.
(24) Wang, D.; Zou, L.; Jin, Q.; Hou, J.; Ge, G.; Yang, L. Human Carboxylesterases: A Comprehensive Review. *Acta Pharm. Sin. B* **2018**, *8*, 699−712.
(25) Lv, X.; Ge, G. B.; Feng, L.; Troberg, J.; Hu, L. H.; Hou, J.; Cheng, H. L.; Wang, P.; Liu, Z. M.; Finel, M.; Cui, J. N.; Yang, L. An Optimized Ratiometric Fluorescent Probe for Sensing Human UDP-Glucuronosyltransferase 1a1 and Its Biological Applications. *Biosens. Bioelectron.* **2015**, *72*, 261−267.
(26) Lv, X.; Zhang, J. B.; Hou, J.; Dou, T. Y.; Ge, G. B.; Hu, W. Z.; Yang, L. Chemical Probes for Human UDP-Glucuronosyltransferases: A Comprehensive Review. *Biotechnol. J.* **2018**, *14*, No. e1800002.
(27) Zhang, L. N.; Ji, K.; Sun, Y. T.; Hou, Y. B.; Chen, J. J. Aurora Kinase Inhibitor Tozasertib Suppresses Mast Cell Activation in Vitro and in Vivo. *Br. J. Pharmacol.* **2020**, *177*, 2848−2859.
(28) Nishi, K.; Kanayama, Y.; Kim, I. H.; Nakata, A.; Nishiwaki, H.; Sugahara, T. Docosahexaenoyl Ethanolamide Mitigates IgE-Mediated Allergic Reactions by Inhibiting Mast Cell Degranulation and Regulating Allergy-Related Immune Cells. *Sci. Rep.* **2019**, *9*, No. 16213.
(29) Ma, R. X.; Hu, J. Q.; Fu, W.; Zhong, J.; Cao, C.; Wang, C. C.; Qi, S. Q.; Zhang, X. L.; Liu, G. H.; Gao, Y. D. Intermittent Fasting Protects against Food Allergy in a Murine Model Via Regulating Gut Microbiota. *Front. Immunol.* **2023**, *14*, No. 1167562.
(30) Lin, J.; Chen, D.; Guan, L.; Chang, K.; Li, D.; Sun, B.; Yang, P.; Liu, Z. House Dust Mite Exposure Enhances Immune Responses to Ovalbumin-Induced Intestinal Allergy. *Sci. Rep.* **2022**, *12*, No. 5216.
(31) Sang, Y. L.; Pannecouque, C.; De Clercq, E.; Wang, S.; Chen, F. E. Picomolar Inhibitor of Reverse Transcriptase Featuring Significantly Improved Metabolic Stability. *Acta Pharm. Sin. B* **2023**, *13*, 3054−3066.
(32) Kim, B.; Kim, R.; Kim, H. J.; Kim, Y.; Park, S. J.; Lee, E. H.; Kim, J.; Kim, J.; Choi, J. W.; Park, J. H.; Park, K. D. Optimization and Evaluation of Pyridinyl Vinyl Sulfones as NRF2 Activator for the Antioxidant and Anti-Inflammatory Effects. *Eur. J. Med. Chem.* **2023**, *256*, No. 115433.
(33) Miners, J. O.; Rowland, A.; Novak, J. J.; Lapham, K.; Goosen, T. C. Evidence-Based Strategies for the Characterisation of Human Drug and Chemical Glucuronidation in Vitro and UDP-Glucuronosyltransferase Reaction Phenotyping. *Pharmacol. Ther.* **2021**, *218*, No. 107689.
(34) Li, M.; He, Q.; Yao, L.; Wang, X.; Tang, Z.; Zhu, X.; Lin, H. S.; Xiang, X. Simultaneous Quantification of Propylthiouracil and Its N-B-D Glucuronide by Hplc-Ms/Ms: Application to a Metabolic Study. *Pharmaceuticals* **2021**, *14*, 1194.
(35) Seeling, M.; Pöhnl, M.; Kara, S.; Horstmann, N.; Riemer, C.; Wöhner, M.; Liang, C.; Brückner, C.; Eiring, P.; Werner, A.; Biburger, M.; Altmann, L.; Schneider, M.; Amon, L.; Lehmann, C. H. K.; Lee, S.; Kunz, M.; Dudziak, D.; Schett, G.; Bäuerle, T.; Lux, A.; Tuckermann, J.; Vögtle, T.; Nieswandt, B.; Sauer, M.; Böckmann, R. A.; Nimmerjahn, F. Immunoglobulin G-Dependent Inhibition of Inflammatory Bone Remodeling Requires Pattern Recognition Receptor Dectin-1. *Immunity* **2023**, *56*, 1046.e7−1063.e7.
(36) Parting, O.; Langer, S.; Kuepper, M. K.; Wessling, C.; Li, S.; Braunschweig, T.; Chatain, N.; Maié, T.; Costa, I. G.; Crysandt, M.; Huber, M.; Brümmendorf, T. H.; Koschmieder, S.; Schemionek, M. Therapeutic Inhibition of FcγRIIB Signaling Targets Leukemic Stem Cells in Chronic Myeloid Leukemia. *Leukemia* **2020**, *34*, 2635−2647.
(37) Shu, Z.; Liu, Q.; Xing, C.; Zhang, Y.; Zhou, Y.; Zhang, J.; Liu, H.; Cao, M.; Yang, X.; Liu, G. Viridicatol Isolated from Deep-Sea *Penicillium griseofulvum* Alleviates Anaphylaxis and Repairs the Intestinal Barrier in Mice by Suppressing Mast Cell Activation. *Mar. Drugs* **2020**, *18*, 517.
(38) Matsui, T.; Teruaki, M.; Hirotaka, Y.; Mikito, M.; Hiroyuki, T. Eppikajutsuto Protects against Food Allergy Induced by Ovalbumin in a Murine Model. *Int. Arch. Allergy Immunol.* **2017**, *173*, 71−83.
(39) Bryce, P. J.; Falahati, R.; Kenney, L. L.; Leung, J.; Bebbington, C.; Tomasevic, N.; Krier, R. A.; Hsu, C. L.; Shultz, L. D.; Greiner, D. L.; Brehm, M. A. Humanized Mouse Model of Mast Cell-Mediated Passive Cutaneous Anaphylaxis and Passive Systemic Anaphylaxis. *J. Allergy Clin. Immunol.* **2016**, *138*, 769−779.

https://doi.org/10.1021/acs.jmedchem.4c00354
J. Med. Chem. 2024, 67, 7504−7515